(S)-roscovitine, a CDK inhibitor, decreases cerebral edema and modulates AQP4 and α1-syntrophin interaction on a pre-clinical model of acute ischemic stroke

Cloé Moëlo, Alicia Quillévéré, Lucas Le Roy, Serge Timsit

Received: 26 April 2023 | Revised: 22 August 2023 | Accepted: 7 September 2023

DOI: 10.1002/glia.24477

GLIA

WILEY

RESEARCH ARTICLE

(S)-roscovitine, a CDK inhibitor, decreases cerebral edema and modulates AQP4 and α1-syntrophin interaction on a pre-clinical model of acute ischemic stroke

Cloé Moëlo[1] | Alicia Quillévéré[1] | Lucas Le Roy[1] | Serge Timsit[1,2]

[1]EFS, Université de Bretagne Occidentale, Inserm UMR 1078, GGB, Brest, France

[2]Neurology and Stroke Unit Department, CHRU de Brest, Inserm1078, Université de Bretagne Occidentale, Brest, France

Correspondence
Serge Timsit, Neurology and Stroke Unit Department, CHRU de Brest, Inserm1078, Université de Bretagne Occidentale, Brest, France.
Email: serge.timsit@chu-brest.fr

Funding information
Université de Bretagne Occidentale

Abstract

Cerebral edema is one of the deadliest complications of ischemic stroke for which there is currently no pharmaceutical treatment. Aquaporin-4 (AQP4), a water-channel polarized at the astrocyte endfoot, is known to be highly implicated in cerebral edema. We previously showed in randomized studies that (S)-roscovitine, a cyclin-dependent kinase inhibitor, reduced cerebral edema 48 h after induction of focal transient ischemia, but its mechanisms of action were unclear. In our recent blind randomized study, we confirmed that (S)-roscovitine was able to reduce cerebral edema by 65% at 24 h post-stroke (*t* test, $p = .006$). Immunofluorescence analysis of AQP4 distribution in astrocytes revealed that (S)-roscovitine decreased the non-perivascular pool of AQP4 by 53% and drastically increased AQP4 clusters in astrocyte perivascular end-feet (671%, *t* test $p = .005$) compared to vehicle. Non-perivascular and clustered AQP4 compartments were negatively correlated ($R = -0.78$; $p < .0001$), suggesting a communicating vessels effect between the two compartments. α1-syntrophin, AQP4 anchoring protein, was colocalized with AQP4 in astrocyte endfeet, and this colocalization was maintained in ischemic area as observed on confocal microscopy. Moreover, (S)-roscovitine increased AQP4/α1-syntrophin interaction (40%, MW $p = .0083$) as quantified by proximity ligation assay. The quantified interaction was negatively correlated with brain edema in both treated and placebo groups ($R = -.57$; $p = .0074$). We showed for the first time, that a kinase inhibitor modulated AQP4/α1-syntrophin interaction, and was implicated in the reduction of cerebral edema. These findings suggest that (S)-roscovitine may hold promise as a potential treatment for cerebral edema in ischemic stroke and as modulator of AQP4 function in other neurological diseases.

KEYWORDS
Aquaporin-4, CDK inhibitor, edema, ischemic stroke, α1-syntrophin

Abbreviations: AQP4, aquaporin 4; BBB, blood–brain barrier; CDK, cyclin-dependent kinases; DAPC, dystrophin associated protein complex; GFAP, glial fibrillary acidic protein; MCA, middle cerebral artery; MW, Mann–Whitney; NVU, neurovascular unit; OAP, orthogonal arrays of particles; PFA, paraformaldehyde; ROI, regions of interest; tMCAo, transient middle cerebral artery occlusion.

1 | INTRODUCTION

Stroke affects 13.7 million people each year and 5.5 million are fatal, ranking it as the second leading cause of death worldwide (Collaborators, 2019; Lindsay et al., 2019). Ischemic stroke caused by arterial occlusion accounts for 80% of all stroke cases. Cerebral edema is a life-threatening complication of middle cerebral artery (MCA) ischemic infarction, occurring in 1%–10% of patients (Wu et al., 2018). The accumulation of cerebrospinal fluid and blood in brain tissue increases intracranial pressure and therefore aggravates ischemia and neurological deterioration. Almost 80% of malignant cerebral edema patients die from its consequences (Huttner & Schwab, 2009). Unfortunately, no effective medical treatment for cerebral edema is available and therapeutic solution against stroke in general are limited in time and options.

We previously showed in double-blind studies on experimental ischemic stroke rat model that (S)-roscovitine was able to dramatically decrease brain edema by 37% to 50%, depending on experimental conditions (Le Roy et al., 2020; Rousselet et al., 2018). (S)-roscovitine is a cyclin-dependent kinase competitive inhibitor (CDKi) targeting mitotic CDKs as CDK 1, 2, 7 and 9 and a particular CDK5, a key mediator of neuronal viability (Bach et al., 2005). CDK5 activity is tightly regulated by its activator protein p35, which is cleaved by calpain under neurotoxic conditions to generate a more stable activator, p25, increasing CDK5 activity. CDK5 hyperactivation during ischemic stroke has been associated with the worst neurological outcome, increased infarct size, neuronal death (Menn et al., 2010) and astrocyte reactivity, and its inhibition has been associated with decreased edema (Le Roy et al., 2021). The beneficial effects of (S)-roscovitine on brain edema depends on its pleiotropic effect on several cellular components of the neurovascular unit (NVU) which protect BBB integrity (Le Roy et al., 2020). Principal component analysis of the NVU cells in relation to edema showed a positive correlation between edema and astrogliosis (Le Roy et al., 2020).

Cerebral edema forms in three successive stages: the early cytotoxic edema phase, quickly followed by the ionic edema phase, and finally the most critical vasogenic edema phase (Clement et al., 2020; Michinaga & Koyama, 2015; Simard et al., 2007; Stokum et al., 2016). Cytotoxic edema is characterized by the swelling of cells surrounding brain vessels within minutes after stroke. Although it does not cause tissue swelling, cytotoxic edema creates an ionic gradient between brain and blood compartments, resulting in subsequent ionic edema with brain swelling (Badaut et al., 2011; Risher et al., 2009). Ionic edema is facilitated by the overexpression of water channels around blood vessels, called aquaporins, and is followed by blood–brain barrier (BBB) rupture and vasogenic edema.

Aquaporin 4 (AQP4) is the most abundant water channel in the central nervous system and plays a crucial role in maintaining cerebral water balance (Bi et al., 2017). AQP4 is mainly expressed in astrocytes and ependymal cells lining the ventricles, with the highest expression on perivascular astrocytes end feet that surround blood vessels (Zelenina, 2010). The highly polarized expression on endfeet (rather than the soma) and the fact that brain endothelial cells are practically devoid of water channels suggests that AQP4 is the main actor of fluid exchanges between the brain and the blood (Patabendige et al., 2021; Søren Nielsen et al., 1997; Verkman et al., 2017). As AQP4 allows passive bidirectional fluid exchanges, water movement is dependent on the difference of osmotic pressure between intra and extracellular space, however, changes in the level of AQP4 expression at the membrane can lead to an increase or a decrease in water permeability of astrocyte membrane. AQP4 channels are anchored to the astrocytic membrane by the dystrophin-associated protein complex (DAPC), a large complex of proteins including dystrophin, dystroglycans and syntrophins that interact with each other and with the cytoskeleton to form a highly organized and stable membrane structure. α1-syntrophin in particular, is thought to play a critical role in regulating both localization and polarization of AQP4 channels in astrocytes (Amiry-Moghaddam et al., 2003; Enger et al., 2012; Neely et al., 2001).

We hypothesized that the anti-edematous effect of (S)-roscovitine could act through the modulation of AQP4.

2 | METHODS

2.1 | Animals

Adult male Sprague–Dawley rats (350 ± 70 g bodyweight) were purchased from Janvier Labs (Le Genest-Saint-Isle, France) and housed in pairs in a temperature-controlled room (21 ± 0.5°C) under a 12-h light/dark cycle. All rats had ad libitum access to food and water. This study was performed in accordance with the European Community Council guidelines on Animal Welfare (2010/63/EU) and approved by the French Ethics Committee for animal experimentation number 74 (reference number: 30334–202103101556826).

2.2 | Surgical procedure

Transient middle cerebral artery (tMCAo) was achieved as previously described (Le Roy et al., 2020; Rousselet et al., 2018). Briefly, rats were anesthetized with 4% and maintained with 1.5% isoflurane in air. Rectal temperature was maintained at 37 ± 0.5°C with a heating pad and a blanket. After cleaning up the surgical area, lurocaine was injected subcutaneously (7 mg/kg) around the incision zone and 2.5 mL of NaCl was injected to prevent dehydration during surgery (Figure 1a). After temporary suture of the common (CCA) and external carotid arteries (ECA) and coagulation of the ECA, a 4–0 monofilament suture (4037PK5Re, Doccol Corporation) was introduced into the right internal carotid artery (ICA) lumen and inserted until resistance was felt (≈ 20 mm) up to the middle cerebral artery (MCA). Neurological score (see below) was measured 90 min after the occlusion following anesthesia recovery. Rats were then anesthetized a second time to take off the monofilament and allow MCA reperfusion. ECA was permanently sutured to avoid blood loss and the temporary suture of CCA was removed; 15 min after reperfusion, either 1.9 mL of vehicle solution (cyclodextrine) or (S)-roscovitine (25 mg/kg) was

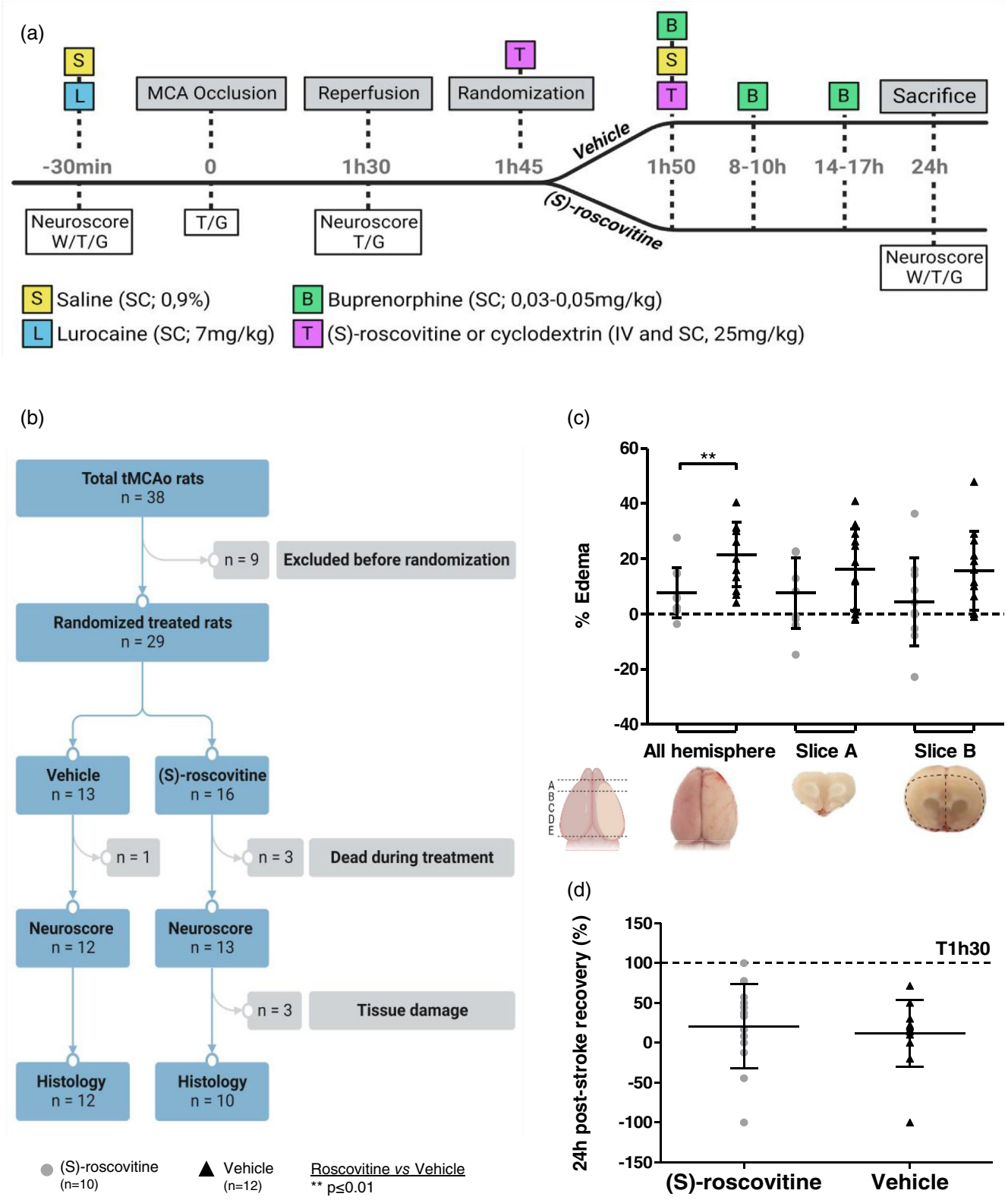

FIGURE 1 Experimental design and effect of (S)-roscovitine, a CDK inhibitor, on cerebral edema (a) Experimental procedure time-lines of a randomized study comparing treated rats ($n = 13$) compared to vehicle ($n = 12$) on a transient focal cerebral ischemia model by middle cerebral artery occlusion (tMCAo). (b) Flow chart. For further experiments, only rats with available histological tissues were studies ($n = 10$ vs. $n = 12$). (c) Decrease of edema volume in whole hemisphere in treated group compared to control (65%, MW, $p = .006$). (d) No difference was observed for recovery between groups at 24 h post-MCAo (MW, $p = .53$). B, buprenorphin; IV, intravenous; L, lurocaine; S, saline; SC, subcutaneous; T, treatment.

TABLE 1 Baseline characteristics.

Body weight (g)	*n*	T0	T24 h
Vehicle	12	333.5 ± 15.3	288.4 ± 14.9
(S)-roscovitine	13	322.8 ± 27.3	298.1 ± 25.8
Unpaired *t* test		ns	ns

Temperature (°C)	T-30 min	T0	T1 h 30 min	T24 h
Vehicle	37.32 ± 0.33	36.90 ± 0.32	37.90 ± 0.88	38.17 ± 0.26
(S)-roscovitine	37.22 ± 0.31	36.95 ± 0.18	37.65 ± 0.96	37.90 ± 0.48
Unpaired *t* test	ns	ns	ns	ns

Glycemia (mg/dL)	T-30 min	T0	T1 h 30 min	T24 h
Vehicle	173.9 ± 13.6	226.5 ± 39.3	174.3 ± 26.5	143.5 ± 18.8
(S)-roscovitine	185.2 ± 14.8	209.5 ± 18.4	172.0 ± 23.4	133.8 ± 18.9
Unpaired *t* test	ns	ns	ns	ns

Note: No difference (MW) between (S)-roscovitine and vehicle-treated rats were observed for temperature, glycaemia and weight at T-30 min, T0, T1 h 30 min and T24 h. Data are expressed as means ± standard deviation.

injected through the jugular vein at a flow rate of 0.48 mL/min, under a randomized repartition. Finally, animals were sutured and a subcutaneous injection of 1.9 mL of the same solution was performed. Postoperative analgesia was administered every 6–12 h to reduce pain (buprenorphine, 0.03–0.05 mg/kg) until sacrifice and softened food was provided. Temperature, blood glucose and weight were monitored during the procedure until sacrifice (Table 1).

2.3 | Exclusion criteria

The following exclusion criteria were used for this study: (1) Rats whose weight was not 310 +/− 40 g before surgery were not included. (2) Rats with total neuroscore <2.5 just before the second anesthesia were immediately excluded and euthanized. (3) Rats which had reached a study endpoint from the care-chart taking in account appearance, behavior and feeding (Table S1) were immediately excluded and euthanized for ethical reasons. (4) Rats that died before the 24 h limit were not included. (5) Rats with no visible infarct in Nissl staining were excluded. A total of 12 vehicle treated rats and 13 (S)-roscovitine treated rats were included in this study (Figure 1b).

2.4 | Neurological scoring procedure

Neurological capacities were assessed before reperfusion at 90′ from ischemia onset and before sacrifice at 24 h post-MCAo according to the modified method developed by Jiang et al. (2005). Neurological score was defined by the sum of two behavioral test scores, the ability of walking without rotating and the reaction to tail suspension, each on a 0-to-4 scale (Table S2). Recovery at 24 h post-MCAo was calculated as a percentage of neurological score decrease from 1 h 30 min post-MCAo as previously described (Rousselet et al., 2018).

2.5 | Brain swelling measurement

Cerebral edema was assessed on whole brain picture, the first 2 mm-slice A and the face of the B slice, obtained with a digital camera (12Mpx camera; resolution 4032 × 3024 dpi). As shown in Data S1 Method 1, measurement of the percentage of edema in whole brain hemispheres and brain frontal slices provides a representative approximation of the global mean edema. The volume of both ipsilesional hemisphere (iH) and contralesional hemisphere (cH) was measured using ImageJ Software in double-blinded conditions. The percentage of brain swelling was then calculated using the Ratios of Ipsilateral and Contralateral Cerebral Hemispheres (RICH) method (Boyko et al., 2019; Kuts et al., 2019; Le Roy et al., 2020; Li et al., 2022; Rousselet et al., 2018; Wali et al., 2012):

$$\text{Brain swelling} = \left[\frac{(\text{Vol iH} - \text{Vol cH})}{\text{Vol cH}}\right] * 100.$$

2.6 | Paraffin embedding

Animals were sacrificed 24 h post-occlusion with intraperitoneal injection of ketamine/xylazine (respectively 80 and 12 mg/kg). To rinse blood vessels, intracardiac perfusion of 200 mL of PBS at 4°C was performed, followed by 200 mL of 4% paraformaldehyde at 4°C (Servilab) to fix tissues. Brains were carefully removed from the skull and placed into a brain matrix to take-off the cerebellum and the olfactory bulb. Whole brains were fixed overnight in 4% PFA at 4°C and rinsed three times in PBS for 15 min each. Tissues were then dehydrated by successive bath of solution with increasing ethanol concentration: 80% for 48–72 h and 100% for 24–48 h. To allow tissues to retain their structure and antigenic sites, brains were processed a 50:50 solutions with 100% ethanol and histochoice solution (Sigma Aldrich) for 12–24 h, and finally 12–24 h in 100% histochoice solution. Paraffin (Sigma Aldrich) was previously melted at 54°C for

24 h to degas the wax. Once dehydrated, tissues were gently placed into molds and embedded in paraffin overnight at 54°C. Half paraffin was replaced with fresh paraffin two times in 24 h and cooled down; 5 µm thick coronal slices were cut with microtome.

2.7 | Immunohistofluorecence staining

Brain slices were dewaxed with two 10-min-baths in histochoice solution before rehydration with incubations in decreasing ethanol concentration starting from 100% ethanol twice for 10 min, 95%, 70% and 50% for 5 min each. Slices were washed in a phosphate-buffered saline (PBS) solution for 10 min and incubated 25 min in citrate buffer solution (95°C) for antibody retrieval and cooled down for 20 min at room temperature. Cell membranes were permeabilized for 30 min in a PBS solution containing 0.3% Triton 100x (PBS-T) and saturated 1 h with a PBS-T solution containing 5% bovine serum albumin (BD Bioscience) to avoid non-specific binding, under gentle agitation. Tissues were then incubated overnight at 4°C with a rabbit polyclonal aquaporin-4 marker (1:500, PA5-78812 Invitrogen), and either a mouse polyclonal glial fibrillary acid protein (GFAP) antibody (1:200, 53-9892-82 Invitrogen) directly conjugated with an Alexa 488 dye, a lectin from *Lycopersicon esculentum agglutinin* (LEA) conjugated with FITC (1:100, L0401 Sigma-Aldrich) or a mouse monoclonal α1-syntrophin antibody (1:100, MA525323 Invitrogen). After being rinsed three times in PBS, slices were incubated for 2 h at room temperature either with a goat anti-rabbit IgG Alexa Fluor 594 secondary antibody (1:500, ab150080 Abcam) for AQP4/GFAP and AQP4/LEA staining or a goat anti-rabbit IgG Alexa Fluor 594 secondary antibody and a goat anti-mouse IgG F(ab′) Alexa Fluor 488^{+} (1:1000, A48286TR Invitrogen) for AQP4/α1-syntrophin staining. Non-specific binding controls are available in Data S1 Methods 2. All antibodies incubations were made under microscopy glass slide ($\oslash = 12$ mm) to prevent evaporation. After being rinsed three times for 5 min under gentle agitation, slices were mounted in a medium with 4′,6-diamidino-2-phenylindole (DAPI Fluoromount-GTM). Observations were made using a Zeiss Axio Imager M2 microscope or a Zeiss Confocal microscope (PIMM UBO Platform).

2.8 | AQP4, GFAP and α1-syntrophin mean fluorescence analysis

Brain slices were entirely scanned on ×10 magnification. In the infarcted hemisphere, "Ischemic core" was identified by an absence of GFAP signal, "Perilesional area" was defined as an area at the border of the ischemic core. Three measures of AQP4 fluorescence were performed by circumventing different structures (cortex or striatum) or conditions (core or perilesional): (i) whole fluorescent intensity for the ischemic core and perilesional area (Figure 2a) either in the cortex or the striatum; (ii) cortex-only fluorescent intensity measures either in the ischemic core or the perilesional area; (iii) striatum-only fluorescent intensity measures either in the ischemic core or the perilesional area. Results were expressed relative to non-ischemic contralateral hemisphere locations: cortex or striatum.

AQP4, GFAP and α1-syntrophin mean intensities were then measured in three regions of interest (ROI) of identical area (0.09 µm^2) in ×40 magnifications and normalized depending on the localization (cortex, striatum) and the severity of ischemia (ischemic core or perilesional area) (Figure 2b). For each condition, the mean of three normalized ROI was calculated as:

$$Normalized\ intensity = \frac{iH\ intensity}{cH\ intensity}.$$

2.9 | GFAP coverage analysis

GFAP surface coverage was also measured on AQP4/GFAP ×40 images in the 3 ROI, using ImageJ software. A fixed automated threshold was defined to determine the percentage of immunoreactive stained surface (coverage). Measures of the ipsilesional hemisphere were normalized with measures of the contralesional hemisphere.

2.10 | AQP4 compartmentation analysis

Compartments analysis was performed on ×40 magnification using the same approach taking in account severity of ischemia (i.e., core or perilesional) and location (i.e., cortex or striatum).

Visual observation of AQP4 distribution staining in the astrocytes allowed to identify three types of distributions of AQP4 fluorescence in the non-ischemic hemisphere that can be separated according to different threshold of fluorescent signal: one non-perivascular at distance from the astrocyte foot and two in the perivascular foot either through diffuse staining along the vessel or through patchy staining along the vessel. These three distribution characteristics were approximated for quantification by defining three threshold according the Gaussian spectra distribution of AQP4 staining: (i) Mean AQP4 intensity-2 standard deviation (M-2SD) area (surface); (ii) (M) to (M + 2SD) area; (iii) > M + 2SD. AQP4 in between (M-2SD) and (M) intensity was identified as "non-perivascular (NP)," AQP4 in between (M) and (M + 2SD) intensity as "perivascular (P)" and finally, AQP4 beyond (M + 2SD) intensity was recognized as "high intensity perivascular clusters (PC)" (Figure 3a).

Images were exported as. CZI files and analyzed using ImageJ (steps available in Data S1 Methods 3). Since images were acquired with three fluorescent channels for AQP4, GFAP and DAPI, the first step was to isolate AQP4 signal by splitting the channels. For each image, the mean and standard deviation were measured to calculate and define three thresholds: (M-2SD), (M) and (M + 2SD). The AQP4 channel image was then triplicated, and each threshold interval was applied to one AQP4 channel image and converted in black and white binary image. White pixels were in the threshold interval while black pixels were outside the threshold. ROI manager tool was then used to

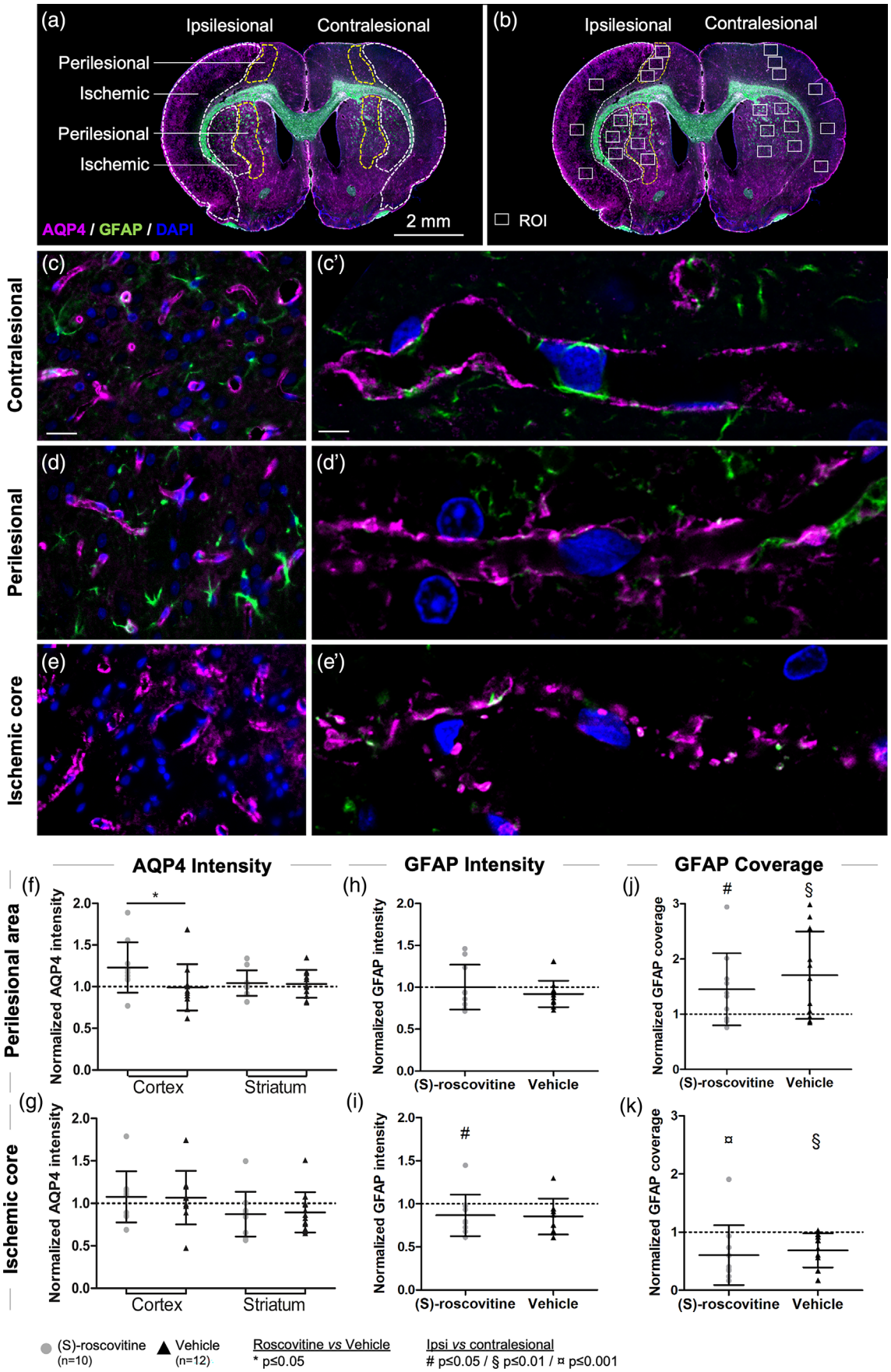

FIGURE 2 Legend on next page.

select all white pixels and measure the selected surface on each image. For normalization the same three contralesional thresholds cut-off were applied to the corresponding ipsilesional ROI as described above (cortex, striatum, perilesional, core). First, analysis was manually done to ensure the reliability of the method, then, it was automatized with an ImageJ macro. Every image of the selection was saved as a checkpoint to control the reliability of the selection.

2.11 | AQP4 fluorescence analysis in brain blood vessels

AQP4 intensity in brain blood vessels was then measured using co-staining with LEA, the most specific lectin to label brain vasculature (Battistella et al., 2021). This analysis was also performed in ×40 magnification using the same approach taking into account severity of ischemia (i.e., core or perilesional) in the cortex and normalized with contralesional measures. For each condition, 10 co-stained blood vessels were selected and analyzed using ImageJ (Data S1 Method 4). Briefly, the LEA image was utilized to create a selection that identifies the blood vessels, and this selection, verified visually, was subsequently applied to the AQP4 image to specifically measure AQP4 intensity within the LEA selection. As the specificity of LEA decreases in pathological condition such as stroke (Battistella et al., 2021), we used a vessel-centered approach instead of using global images to avoid the bias of microglia/macrophages staining.

2.12 | In situ analysis of AQP4 and α1-syntrophin interaction by proximity ligation assay

Brain slices were dewaxed, rehydrated, underwent antigen retrieval process, and were permeabilized and saturated as described in immunofluorescence protocol. Tissues were incubated overnight at 4°C with the same primary antibodies against aquaporin-4 and α1-syntrophin mentioned above, at the same concentrations. After incubation, the slices were washed one time in PBS-T and two times in DPBS (Gibco™) for 5 min each under gentle agitation and incubated 1 h at 37°C with a couple of oligonucleotide-conjugated secondary antibodies PLA Probe anti-mouse MINUS and anti-rabbit PLUS (Sigma Aldrich Duolink) diluted in blocking solution. After three rinses of 5 min with DPBS, the ligation step was performed with ligase diluted in ligation stock for 30 min at 37°C, allowing the hybridization of the two oligonucleotides in the PLA probes with the circular matrix. Tissues were rinsed three times for 5 min in DPBS and incubated for 2 h 30 min at 37°C with polymerase diluted in amplification solution stock, which contains labeled oligonucleotides with Far Red fluorophores (Sigma Aldrich Duolink). This amplification step allows the detection of the interaction between the two proteins. After three rinses of 5 min with DBPS, slices were incubated with GFAP-conjugated AF488 antibody overnight at 4°C to visualize astrocyte end-foot. Finally, tissues were rinsed and mounted in medium containing DAPI. All incubations were made under a microscopy glass slide and in a humidified chamber to prevent evaporation. Observations were made using a Zeiss Axio Imager M2 microscope. PLA dots were quantified using ImageJ software (steps available in Data S1 Methods 5, adapted from (Lopez-Cano et al., 2019) on 10 randomly taken ×63 magnification in the ischemic and the perilesional cortex and normalized with the contralesional cortex. PLA analysis was not performed is the striatum because the natural strong autofluorescence of this region caused artifacts.

2.13 | Statistical analysis

Graph Pad Prism 5 software was used to analyze the data. Gaussian distribution was tested by the Pearson normality test and analyzed by two-tailed unpaired Student's t test. Non-Gaussian distributed variables were analyzed by non-parametric Mann–Whitney test (MW). All data were presented as mean and standard deviation. The alpha level was set at p values less than .05. Pearson correlations analysis were conducted using R-Studio Software "*corrplot*," "*psych*," "*ggplot2*," "*ggpubr*" and "*ggplotify*" packages, for both AQP4/GFAP and PLA/Edema correlation analysis.

3 | RESULTS

3.1 | Baseline characteristics and recovery

Physiological parameters were monitored throughout the tMCAo procedure and until the sacrifice (Table 1). Body temperature was maintained around 37°C during anesthesia and blood glucose was

FIGURE 2 Change in AQP4 expression caused by ischemia is modulated by (s)-roscovitine, which increased AQP4 signal in the perilesional region without affecting astrocytes (a–e′) Immunohistofluorescent analysis on brain coronal sections of tMCAo rats of AQP4 (pink), GFAP (green) and DAPI (blue) staining at low magnification (a,b, ×10), high magnification (c–e, ×40) and in confocal microscopy (c′–e′). (a) Scale bar length is 2 mm. (b) Selection of three region of interest (ROI) for each localization in the ischemic core and perilesional area of the cortex and the striatum, and by symmetry in contralesional hemisphere. In c–e, note the presence of astrocyte GFAP signal (green) in c and d but not in e. Scale bar length is 20 µm. In c′–e′ note the AQP4 continuous signal in the vessel in the contralesional cortex (C′) while AQP4 appeared more diffuse in the perilesional (d′) and more patchy in the core vessels (e′). Scale bar length is 5 µm. (f–g) AQP4 mean fluorescence analysis was performed on ×40 ROI in perilesional (f) and core (g) of both cortex and striatum and normalized with contralesional measurements (dotted line). (S)-roscovitine increased AQP4 signal in perilesional area. (h–k) No difference in GFAP intensity or surface coverage was observed between treated and vehicle groups in perilesional and core of cortex. GFAP coverage significantly increased in perilesional area (j) and significantly decreased in core (k) of both groups. Measurements were performed by a blind operator. Data are expressed as mean ± standard deviation. *$p \leq .05$ (S)-roscovitine versus vehicle; #$p \leq .05$; § $p \leq .01$; ☼$p \leq .001$ ipsilesional versus contralesional.

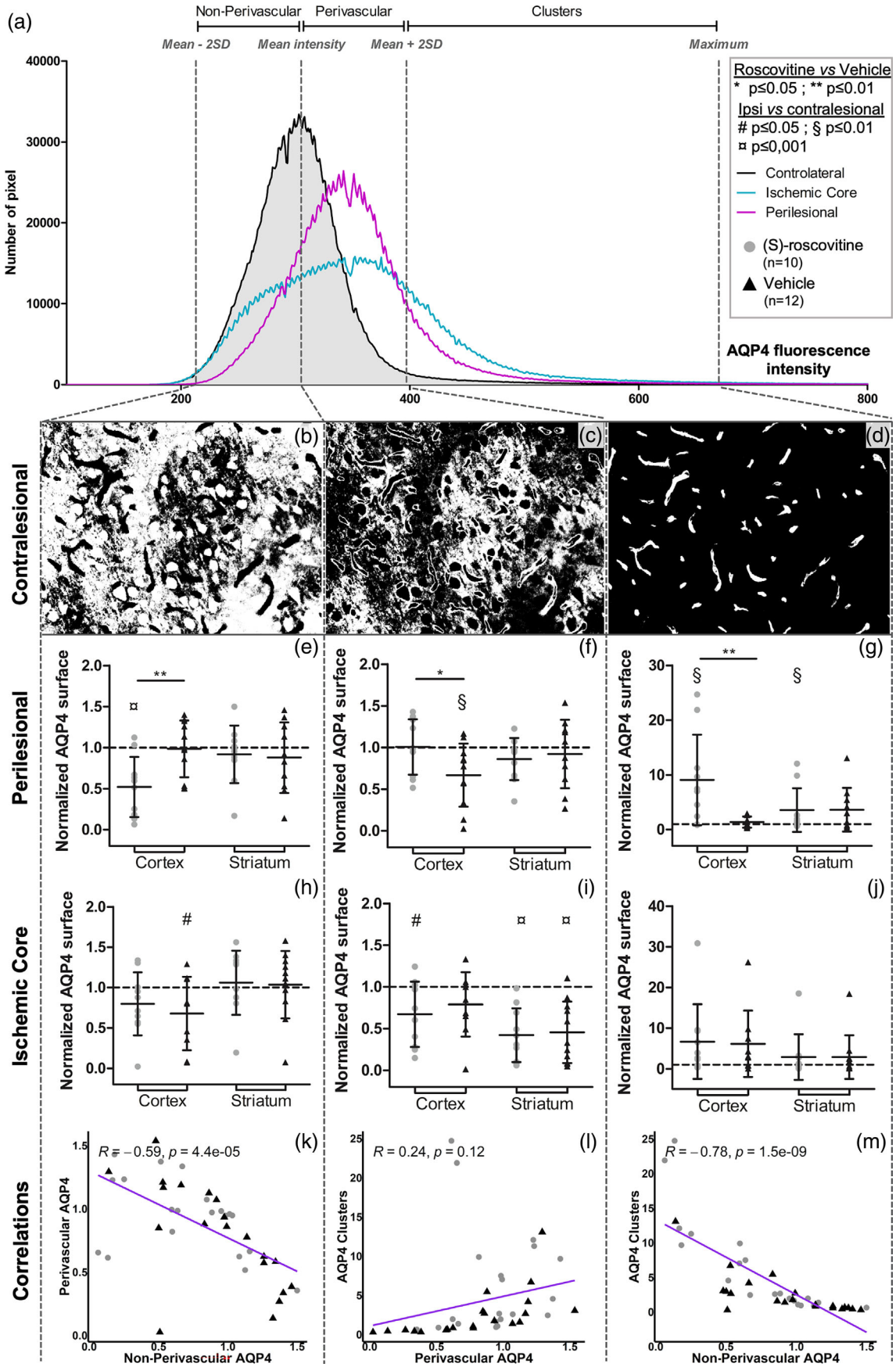

FIGURE 3 Legend on next page.

quantified throughout the procedure, no significant difference was observed between treated and non-treated groups before or after the procedure, and neither on the day of sacrifice. No significant difference in recovery at 24 h post tMCAo was observed between the groups (vehicle: 20.63 ± 52.64 vs. (S)-roscovitine: 11.40 ± 41.90; MW $p = .53$) (Figure 1d).

3.2 | (S)-roscovitine reduced cerebral edema

(S)-roscovitine reduced by 65% the volume of cerebral edema 24 h after MCAo, as measured on whole hemispheres (vehicle: 21.49 ± 11.71% vs. (S)-roscovitine: 7.67 ± 9.04%; *t* test $p = .006$; Figure 1c). Edema volume on frontal slices tended also to be reduced in the (S)-roscovitine group, for both slice A (vehicle: 16.2 ± 14.7% vs. (S)-roscovitine: 7.6 ± 12.9%; *t* test $p = .16$) and slice B (vehicle 15.6 ± 14.3% vs. (S)-roscovitine: 4.4 ± 15.9%; *t* test $p = .1$).

3.3 | AQP4 distribution changed in the ischemic brain

To illustrate the consequences of a stroke on AQP4 repartition around blood vessels, optic ×40 and confocal ×63 magnification ROI were analyzed (Figure 2b). In contralesional hemisphere, AQP4 signal was highly polarized at the perivascular astrocyte end-foot (Figure 2c,c′). In perilesional area, AQP4 signal in blood vessels showed a redistribution of AQP4 expression in non-perivascular astrocyte membrane, resulting in a less polarized pattern of expression and a more diffuse perivascular expression (Figure 2d,d′). In the ischemic core, a fragmented AQP4 staining was observed at the BBB (Figure 2e,e′).

3.4 | (S)-roscovitine increased AQP4 fluorescence intensity independently of astrocytes GFAP signal

AQP4 fluorescence analysis of the perilesional area at low magnification (×10) showed a significantly higher signal in the (S)-roscovitine treated group (vehicle: 0.91 ± 0.11 vs. (S)-roscovitine: 1.07 ± 0.24; MW $p = .0132$) (data not shown). (S)-roscovitine increased significantly AQP4 fluorescence intensity in the striatum (vehicle: 0.93 ± 0.096 vs. (S)-roscovitine: 1.05 ± 0.15; *t* test $p = .0483$) and tended to increase it in the cortex (vehicle: 0.88 ± 0.29 vs. (S)-roscovitine: 1.08 ± 0.29; *t* test $p = .10$). (S)-roscovitine group presented a similar level of AQP4 in ischemic core and in contralesional hemisphere whereas vehicle group showed a significantly lower AQP4 fluorescence intensity (vehicle: 0.85 ± 0.13 vs. (S)-roscovitine: 0.97 ± 0.21; MW $p = .045$), and more specifically in the cortex (vehicle: 0.85 ± 0.15 vs. (S)-roscovitine: 1.02 ± 0.19; MW $p = .0489$) (data not shown).

At higher magnification (×40), AQP4 fluorescence intensity was increased in (S)-roscovitine perilesional cortex compared to vehicle group (vehicle: 0.99 ± 0.28 vs. (S)-roscovitine: 1.23 ± 0.3; MW $p = .02$) (Figure 2f), but not in the striatum. No significant difference between vehicle and (S)-roscovitine groups on the infarct zone was observed at ×40 magnification (Figure 2g).

GFAP fluorescence intensity did not change with (S)-roscovitine treatment (Figure 2h,i). GFAP coverage was significantly increased in perilesional area of (S)-roscovitine group (MW $p = .012$; Figure 2j) and decreased in ischemic core (vehicle: MW $p = .0049$; (S)-roscovitine: MW $p = .0005$; Figure 2k) for both groups compared to contralesional, no significant difference was observed between (S)-roscovitine and vehicle groups.

3.5 | (S)-roscovitine increased AQP4 polarization in perilesional area

The following results in perilesional zone and ischemic core are normalized with contralesional measurements, represented as a dotted line on the graphs.

(S)-roscovitine changed AQP4 repartition in perilesional cortex. A significant 48% decrease in non-perivascular (NP) AQP4 surface was observed in (S)-roscovitine perilesional cortex compared to contralesional cortex (*t* test $p = .0002$), while no change was reported in vehicle group, resulting in a significant difference between the two groups (vehicle: 0.98 ± 0.34 vs. (S)-roscovitine: 0.52 ± 0.37; *t* test $p = .0076$) (Figure 3e). Perivascular (P) AQP4 surface significantly decreased in the vehicle perilesional cortex compared to contralesional (*t* test; $p = .008$) while no change was observed in (S)-roscovitine group (vehicle: 0.67 ± 0.38 vs. (S)-roscovitine: 1.01 ± 0.33; *t* test $p = .042$;

FIGURE 3 Effect of (S)-roscovitine on astrocyte end-foot AQP4 compartmentation after ischemic stroke (a) Graphical representation of AQP4 fluorescence Gaussian distribution on ×40 magnifications in contralesional (gray), perilesional area (purple) and ischemic core (blue). X-axis shows fluorescence intensity while Y-axis shows the number of fluorescent pixels. Three thresholds have been defined, depending on the mean fluorescence (M) and the standard deviation (SD), as: (M-2SD), (M) and (M + 2SD), separating three compartments: Non-perivascular (NP), Perivascular (P) and Clusters (PC). P and PC are located at the vessel on the astrocyte end-foot. (b–d) Fluorescent microscopy image of contralateral hemisphere for the three applied thresholds. White pixels represent the area selected by the threshold while black pixels are excluded by the threshold. (e–j) Cortical and striatal AQP4 repartition between non perivascular, perivascular and AQP4 clusters compartments in ischemic core (e–g) and in perilesional zone (h, i). (S)-roscovitine significantly decreased non-perivascular AQP4 surface and increased by a factor 9 AQP4 clusters in the perilesional cortex. No effect of the treatment was measured in the core. Measurements were performed with an automatized ImageJ program. Data are expressed as mean ± standard deviation. $^{*}p \leq .05$; $^{**}p \leq .01$ (S)-roscovitine versus vehicle group. $\#p \leq .05$; $\S p \leq .01$; $\divideontimes p \leq .001$ ipsilateral versus contralateral. (k–m) Pearson correlation between AQP4 compartments was analyzed with R-Studio. A significant negative correlation was observed between NP and both P (k) and PC (m).

Figure 3f). (S)-roscovitine significantly increased the surface area of AQP4 high-intensity clusters (PC) by a factor of nine (*t* test; $p = .004$) in the perilesional cortex compared to the contralesional cortex, whereas no change was observed in the vehicle group (vehicle: 1.35 ± 1.02 vs. (S)-roscovitine: 9.06 ± 8.29; *t* test $p = .005$; Figure 3g). No significant effect of (S)-roscovitine on AQP4 repartition was observed in the perilesional striatum. No significant difference between vehicle and (S)-roscovitine groups on the ischemic core was observed (Figure 3h–j). The comparison of contralesional and ischemic territories revealed for both group a significant reduction of AQP4-P surface in cortex (vehicle: *t* test $p = .08$; (S)-roscovitine: *t* test $p = .01$) and striatum (vehicle: *t* test $p < .0001$; (S)-roscovitine: *t* test $p = .0003$; Figure 3i).

Correlations were computed to highlight the relationship between NP, P and PC compartments. Results showed that NP AQP4

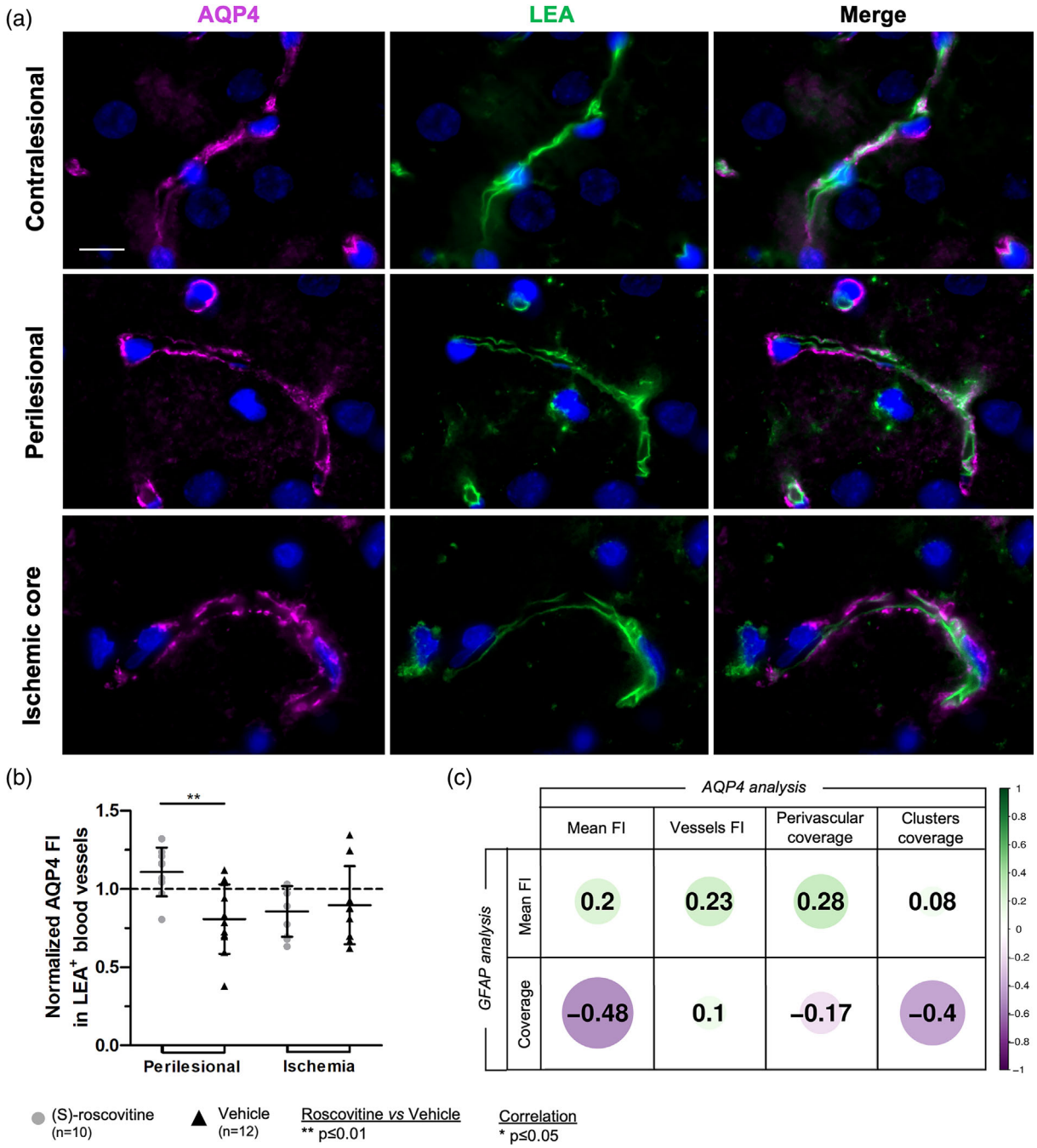

FIGURE 4 (S)-roscovitine enhances AQP4 expression in blood vessels in perilesional area. (a) Immunohistofluorescent analysis of AQP4 (pink) and Lycopersicon esculentum agglutinin LEA (green) in contralesional, perilesional and ischemic core blood vessels in the cortex. Scale bar length is 10 µm. (b) AQP4 fluorescence intensity (FI) was measured in LEA+ blood vessels of the different regions using ImageJ. (S)-roscovitine significantly increased AQP4 signal in perilesional area (*t* test; $p = .003$). (c, d) Pearson correlation between AQP4 global and vessels-specific FI and GFAP FI and coverage was analyzed using RStudio. No significant correlation was found in perilesional area. A significant negative correlation was observed between GFAP FI and AQP4 vessels-specific signal.

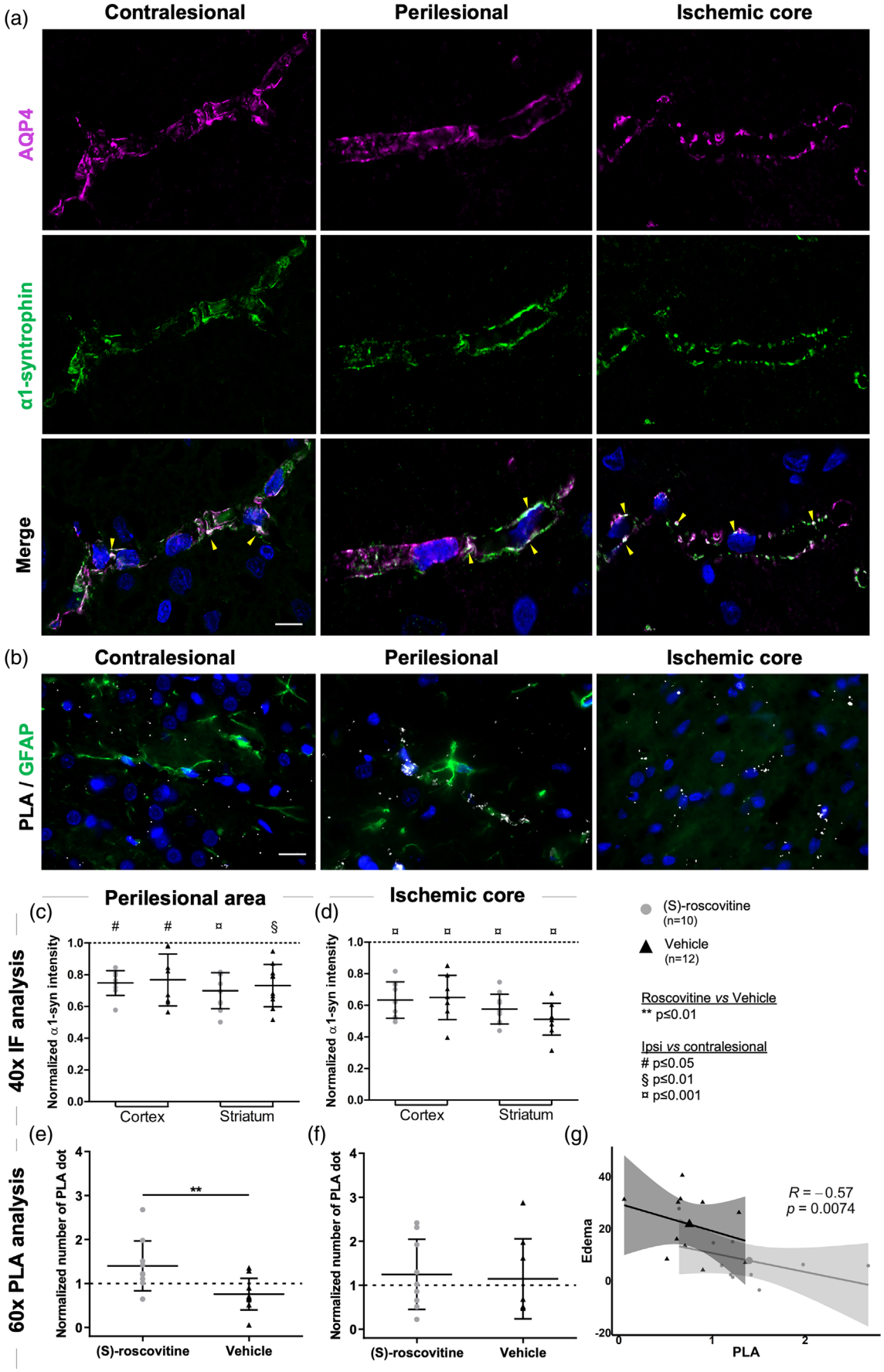

FIGURE 5 Legend on next page.

compartment was negatively correlated with AQP4-P ($R = -.59$; $p < .0001$; Figure 3k) and strongly negatively correlated with AQP4-PC compartment ($R = -.78$; $p < .0001$; Figure 3m), in both groups. PC and P compartments trended to be positively correlated ($R = .24$; $p = .12$).

3.6 | Vascular AQP4 increased fluorescence signal evidenced by vasculature staining

A co-staining with the vascular-label LEA lectin was then performed to confirm the increase in AQP4 in blood vessels (Figure 4a). LEA staining was visible on vessels, that is, endothelial cells, with AQP4 staining but also on microglia/macrophages without AQP4 staining. LEA signals were observed in contralesional, perilesional and ischemic regions and exhibited continuous labeling of blood vessels, which notably contrasted with the irregular staining pattern of AQP4 in the ischemic core. Measure of AQP4 fluorescence intensity specifically in LEA-positive blood vessels using a vessel-centered approach (see above) showed a significant increase in the perilesional area of (S)-roscovitine group compared to vehicle group (vehicle: 0.80 ± 0.22 vs. (S)-roscovitine: 1.11 ± 0.15; *t* test $p = .003$) (Figure 4b).

3.7 | AQP4 increase by (S)-roscovitine is not related to a higher astrocyte reactivity

Correlations were calculated between on the one hand, GFAP for Mean fluorescence intensity (FI) or coverage, and, on the other hand, AQP4 for Mean FI, vessel FI (as defined by LEA), perivascular and clusters coverage. No significant positive correlation but rather negative correlation was found (Figure 4c).

3.8 | AQP4 and α1-syntrophin colocalization is maintained in perilesional and ischemic brain

×40 magnification analysis of α1-syntrophin expression showed a perivascular distribution in contralesional hemisphere, the perilesional area and ischemic core. Confocal analysis of α1-syntrophin (green) and AQP4 (pink) co-distribution revealed a strong colocalization in the vessel wall, visible in white and pointed at with arrows in merge images, in each ROI (Figure 5a). This co-distribution was also assessed with PLA technique, revealing a preserved interaction between AQP4 and α1-syntrophin in ischemic regions (Figure 5b).

3.9 | Ischemia reduces α1-syntrophin fluorescence intensity

In both (S)-roscovitine and vehicle groups, α1-syntrophin mean fluorescence intensity was significantly reduced by ∼25% in the perilesional cortex (vehicle: *t* test $p = .028$; (S)-roscovitine *t* test $p = .011$) and by ∼30% in the perilesional striatum (vehicle: *t* test $p = .002$; (S)-roscovitine *t* test $p < .0001$) compared to contralesional (Figure 5c). α1-syntrophin was also reduced by ∼35% in the cortical ischemic core for both groups (vehicle: *t* test $p = .0003$; (S)-roscovitine *t* test $p < .0001$; Figure 5d). In the striatum ischemic core, α1-syntrophin intensity decreased by 42% in the (S)-roscovitine group (*t* test $p < .0001$) and by 49% in the vehicle group (MW $p < .0001$). No significant difference in α1-syntrophin fluorescence was observed between the two groups.

3.10 | (S)-roscovitine enhances AQP4 and α1-syntrophin interaction in perilesional area

(S)-roscovitine enhanced by 40% AQP4 and α1-syntrophin interactions detected in PLA in the perilesional cortex (vehicle: 0.75 ± 0.38 vs. (S)-roscovitine: 1.40 ± 0.57; MW $p = .0083$; Figure 5e). No significant difference was observed between the two groups in the cortical ischemic core (Figure 5f).

The interaction between AQP4 and α1-syntrophin was negatively correlated with the brain swelling in both groups ($R = -.57$; $p = .0074$; Figure 5g). Notably, the (S)-roscovitine group exhibited a higher number of PLA dots associated with less edema, while the vehicle group showed a lower number of PLA dots associated with more cerebral edema.

4 | DISCUSSION

In this blind randomized study, we investigated the effect of CDK inhibitor, (S)-roscovitine on AQP4 and α1-syntrophin expression with

FIGURE 5 Co-distribution of α1-syntrophin and AQP4 at perivascular astrocytic end-foot: (S)-roscovitine enhances AQP4-α1-syntrophin interaction in perilesional area and is correlated with edema (a) Confocal view of AQP4 (pink) and α1-syntrophin (green) co-distribution in contralesional, perilesional and ischemic core blood vessels. Note the colocalization of AQP4 and α1-syntrophin, noticeable in white on merge images (arrows), in the contralesional cortex and also in perilesional area and ischemic core. Scale bar length is 10 μm. (b) ×63 magnification of GFAP staining (green), DAPI (blue) and Proximity Ligation Assay (PLA) dots (white) of AQP4/α1-syntrophin in contralesional, perilesional and ischemic core. Scale bar length is 10 μm. α1-syntrophin mean fluorescence intensity was measured on ×40 magnification and normalized (dotted line) in perilesional area (c) and ischemic core (d) of cortex and striatum. A significant reduction of α1-syntrophin fluorescence was measured in both regions, but no effect of (S)-roscovitine was observed. (e, f) PLA dots were automatically counted on ×63 magnification with ImageJ program and normalized (dotted line). (S)-roscovitine increased the number of PLA dots detected in perilesional area. Data are expressed as mean ± standard deviation. $^{**}p \leq .01$ (S)-roscovitine versus vehicle group. $\#p \leq .05$; $\S p \leq .01$; $\star p \leq .001$ ipsilateral versus contralateral. (g) Significant negative Pearson correlation between edema and perilesional PLA data.

an intraluminal filament tMCAo rat model, the reference model for pre-clinical studies of acute ischemic stroke treated by endovascular thrombectomy (Sutherland et al., 2016). Our main results are that (S)-roscovitine decreased cerebral edema, modulated AQP4 polarization, and that this modulation was dependent upon α1-syntrophin.

4.1 | (S)-roscovitine decreases cerebral edema at 24H

Our results showed that (S)-roscovitine administration 90 min after ischemia onset induced a significant 65% reduction of cerebral edema at 24 h post-stroke. (S)-roscovitine was previously shown to decrease brain edema by 37% to 50% in randomized blind studies on 90 min tMCAo rat models at 48 h post-stroke (Le Roy et al., 2020; Rousselet et al., 2018). To our knowledge, this is the first observation of an anti-edematous effect of (S)-roscovitine 24 h post-stroke, showing an early modulation of brain swelling by CDK inhibitor. This edema decrease was not associated with neurological recovery 24 h post-stroke in treated group, although previous studies showed that (S)-roscovitine administration improved neurological score 24 and 48 h after tMCAo (Le Roy et al., 2020; Menn et al., 2010; Rousselet et al., 2018). Maybe the difference is due the time of analysis, suggesting that it take time for edema reduction to improve clinical score. Another explanation may be related to the sensitivity of clinical score to detect subtle recovery.

4.2 | (S)-roscovitine modulates AQP4 polarization and its different compartments, enhancing AQP4 expression at the vessel, independently of astrocyte reactivity in ischemic tissue

In non-ischemic regions, qualitative analysis of AQP4 expression in confocal microscopy showed, as expected (Hubbard et al., 2015), that AQP4 was highly polarized and homogenously distributed in astrocyte perivascular end-feet. In ischemic regions, change in AQP4 expression was observed at 24 h post-occlusion in core and perilesional areas: a loss of polarization was noticed in the perilesional zone, with AQP4 signal spreading in the astrocyte membrane and a fragmented pattern was observed in blood vessel walls of ischemic core as previously reported in others cerebral infarction models such as multiple microinfarcts, traumatic brain injury and subarachnoid hemorrhage (Fang et al., 2020; Ren et al., 2013; Wang et al., 2012). Furthermore, a significant reduction of AQP4 expression was already observed (Frydenlund et al., 2006), in the ischemic core of vehicle animals compared to contralateral non-ischemic side.

(S)-roscovitine treatment analysis showed an effect on both AQP4 polarization and level of expression after ischemia. In perilesional cortex, (S)-roscovitine significantly decreased non-perivascular AQP4 and drastically increased AQP4 clusters in astrocyte perivascular end-feet. The correlation analysis showed that the cluster compartment and the perivascular compartment were significantly and negatively correlated with the non-vascular compartment (Figure 3). On the contrary, no correlation was observed between cluster and perivascular compartments.

To determine whether AQP4 polarization was not a result of increased astrocytes reactivity observed after a stroke, we studied the relationship between AQP4 and GFAP signals. The effect of (S)-roscovitine on AQP4 expression was not associated with any impact on astrocytes, as there were no differences in GFAP intensity or coverage between both groups, and no correlation was found between GFAP and AQP4 signals. Furthermore, our previous study showed that (S)-roscovitine significantly reduced both astrocyte number and GFAP intensity 48 h post-stroke (Le Roy et al., 2020), and we observed, at 24 h, although not significantly, rather a negative correlation as expected from previous work (Figure 4c).

To confirm change in AQP4 localization at the astrocyte end-foot with (S)-roscovitine we co-labeled the ischemic tissue with a vascular marker—that is, LEA lectin—and AQP4. The experiment showed that (S)-roscovitine treatment significantly increased AQP4 signal in LEA+ vessels (Figure 4b). Qualitative assessment of vasculature with LEA lectin showed a continuous signal along the blood vessels, contrasting with the irregular clustered pattern of AQP4 in the ischemic score suggesting that the change in AQP4 expression at the astrocyte end-foot is not driven by endothelial demise.

These observations strongly suggest that there is an "interconnected compartmentalization" of different pools of AQP4 more than a direct modulation of AQP4 induced by the treatment, as alterations in the perivascular pool of AQP4 seem to have an impact on the non-perivascular pool of AQP4, in such a way that an increase in one compartment leads to a decrease in another compartment. The effect of (S)-roscovitine on AQP4 is observed on ischemic tissue; its effect on healthy tissue remains to be determined. A recent study conducted on 90 min-occlusion tMCAo rats reported that AQP4 level of expression in the non-ischemic hemisphere was similar to AQP4 expression in sham (Murata et al., 2020), suggesting that under the conditions of our study, AQP4 seems to remain stable in the non-ischemic hemisphere.

The polarized distribution of AQP4 in the brain is important for regulating water transport in both normal and pathological conditions (Kitchen et al., 2020; Manley et al., 2004; Nakada, 2014), with evidence indicating that vascular polarized AQP4 expression is more important for effective fluid transport, rather than total AQP4 levels in the tissue (Gomolka et al., 2023; Hablitz et al., 2020; Mestre et al., 2018; Sylvain et al., 2021). It is also noteworthy that the effect of (S)-roscovitine took place in the cortex but did not impact the striatum where AQP4 is more diffusely expressed in astrocyte processes, suggesting that AQP4 expression is regulated in a region-specific manner which may be related to the functional differences of astrocytes in different brain regions (Aoyama et al., 2012; Guo et al., 2021).

4.3 | AQP4 polarization is dependent upon α1-syntrophin for localization and roscovitine modify AQP4/α1-syntrophine interaction directly or indirectly

Since α1-syntrophin is a cytoplasmic protein that binds directly or indirectly to the C-terminus of AQP4 channels, and this interaction allows AQP4 addressing and anchoring at astrocyte endfeet (Amiry-Moghaddam

et al., 2003; Enger et al., 2012; Neely et al., 2001; Peters et al., 1997), we studied the joint expression of AQP4 and α1-syntrophin.

Confocal microscopy showed that α1-syntrophin and AQP4 expression profile were co-localized with a high polarization around blood vessels in non-ischemic territories and a fragmented pattern in ischemic core. The colocalization of the two proteins in astrocyte end-feet observed in non-ischemic tissue was maintained in perilesional and ischemic tissue. However, despite a loss of AQP4 polarization in perilesional area, α1-syntrophin was still exclusively expressed in astrocyte perivascular end-feet. Fluorescence analysis of α1-syntrophin showed a lower intensity in ischemic territories compared to non-ischemic hemisphere, but no difference was measured between (S)-roscovitine and vehicle groups. Amiry-Moghaddam et al. previously observed similar change of AQP4 and α1-syntrophin expression in a 90 min tMCAo mice model after 23 h reperfusion (Amiry-Moghaddam et al., 2003). They hypothesized that AQP4 loss of polarization was not due to a breakdown of membrane integrity because α1-syntrophin was still perivascular, but rather due to an alteration of the link between α1-syntrophin and AQP4.

Quantification of AQP4 and α1-syntrophin interactions using proximity ligation assay (PLA) showed that (S)-roscovitine increased this interaction in perilesional area compared to vehicle. Furthermore, for both treated and placebo group, AQP4 and α1-syntrophin interactions in the perilesional area was negatively correlated with brain edema. This data shows that (S)-roscovitine modulates the interaction between AQP4 and α1-syntrophin and that this interplay is instrumental in cerebral edema in both treated and non-treated group. However, it remains to be determined whether (S)-roscovitine acts directly or indirectly on AQP4/α1-syntrophin complex.

Since (S)-roscovitine is a kinase inhibitor with a high number of phosphoryl table targets (Bach et al., 2005), it is possible that this AQP4/α1-syntrophin interaction depends on a phosphorylation mechanism and especially CDK5 phosphorylation since (S)-roscovitine has an IC50 < 1 μm for CDK5. AQP4 and α1-syntrophin possess multiple phosphorylation sites, some of which may be dependent upon CDK5. Interestingly, there is a reported CDK5 phosphorylation site near the PDZ domain of α1-syntrophin, which is likely involved in targeting or stabilizing AQP4 (Adams et al., 2001; Neely et al., 2001). In pancreatic β-cells, the PDZ domain of β2-syntrophin regulates the release of insulin and helps in maintaining the blood glucose level. When CDK5 phosphorylates the β2-syntrophin on Ser75 near the PDZ domain, it decreases its binding to insulin granules and increases its motility and exocytosis (Ort et al., 2001; Schubert et al., 2010). A similar phenomenon could be observed in AQP4/α1-syntrophin interaction.

Many studies suggest that AQP4 has different roles in development and resolution of cerebral edema, with water flow through AQP4 driving cytotoxic edema development in the early post-injury stage but later clearing vasogenic edema. Consequently, reversible modulation of AQP4 function during the acute phase is a viable strategy to prevent CNS edema. However, despite intense efforts over many years, no water-channel-blocking drugs for any AQP have been approved for use in humans (Patabendige & Chen, 2022).

To our knowledge this is the first time that a kinase inhibitor was shown to modify in vivo AQP4 polarization and its different pools in astrocytes, but also to modulate AQP4/α1-syntrophin interaction. This interaction plays a key role in cerebral edema but also in other neurological diseases such as Alzheimer disease (Simon et al., 2022) or dystrophinopathies (Colvin et al., 2022). Hence, (S)-roscovitine, and others cyclin-dependent kinase inhibitors, may represent a new class of drugs for targeting AQP4/α1-syntrophin dysfunctions.

AUTHOR CONTRIBUTIONS

Serge Timsit supervised the project. Cloé Moëlo and Serge Timsit designed the study concept. Cloé Moëlo performed all experiments. Alicia Quillévéré trained Cloé Moëlo for proximity ligation assay. Lucas Le Roy trained Cloé Moëlo for animal model of stroke and immunofluorescence. Cloé Moëlo and Serge Timsit analyzed the data and wrote the first draft. All authors read and approved the final version of the manuscript.

ACKNOWLEDGMENTS

The authors thank Dr Marc Blondel (Astre, INSERM 1078 GGB) for his helpful suggestions, Dr Ozvan Bocher (Institute of Translational Genomics, Munich) and Marie-Sophie Ogloblinski (BIGG, INSERM U1078 GGB) for their support in statistical analysis and programming, Philippe Elies (PIMM, Université de Bretagne Occidentale) for technical support and image analysis advice and Severine Loisel, Marie-Françoise Scoazec and Manuel Feillant (Animalerie Commune, Université de Bretagne Occidentale) for their assistance with animal care.

CONFLICT OF INTEREST STATEMENT

The authors declare no competing interests.

DATA AVAILABILITY STATEMENT

Research data are not shared.

ORCID

Serge Timsit https://orcid.org/0000-0003-0346-8576

REFERENCES

Adams, M. E., Mueller, H. A., & Froehner, S. C. (2001). In vivo requirement of the alpha-syntrophin PDZ domain for the sarcolemmal localization of nNOS and aquaporin-4. *The Journal of Cell Biology*, *155*(1), 113–122. https://doi.org/10.1083/jcb.200106158

Amiry-Moghaddam, M., Otsuka, T., Hurn, P. D., Traystman, R. J., Haug, F. M., Froehner, S. C., Adams, M. E., Neely, J. D., Agre, P., Ottersen, O. P., & Bhardwaj, A. (2003). An alpha-syntrophin-dependent pool of AQP4 in astroglial end-feet confers bidirectional water flow between blood and brain. *Proceedings of the National Academy of Sciences of the United States of America*, *100*(4), 2106–2111. https://doi.org/10.1073/pnas.0437946100

Aoyama, M., Kakita, H., Kato, S., Tomita, M., & Asai, K. (2012). Region-specific expression of a water channel protein, aquaporin 4, on brain astrocytes. *Journal of Neuroscience Research*, *90*(12), 2272–2280. https://doi.org/10.1002/jnr.23117

Bach, S., Knockaert, M., Reinhardt, J., Lozach, O., Schmitt, S., Baratte, B., Koken, M., Coburn, S. P., Tang, L., Jiang, T., Liang, D. C., Galons, H., Dierick, J. F., Pinna, L. A., Meggio, F., Totzke, F., Schächtele, C.,

Lerman, A. S., Carnero, A., … Meijer, L. (2005). Roscovitine targets, protein kinases and pyridoxal kinase. *The Journal of Biological Chemistry*, *280*(35), 31208–31219. https://doi.org/10.1074/jbc.M500806200

Badaut, J., Ashwal, S., & Obenaus, A. (2011). Aquaporins in cerebrovascular disease: a target for treatment of brain edema? *Cerebrovascular Diseases*, *31*(6), 521–531. https://doi.org/10.1159/000324328

Battistella, R., Kritsilis, M., Matuskova, H., Haswell, D., Cheng, A. X., Meissner, A., Nedergaard, M., & Lundgaard, I. (2021). Not all lectins are equally suitable for labeling rodent vasculature. *International Journal of Molecular Sciences*, *22*(21), 11554. https://doi.org/10.3390/ijms222111554

Bi, C., Tham, D. K. L., Perronnet, C., Joshi, B., Nabi, I. R., & Moukhles, H. (2017). The oxidative stress-induced increase in the membrane expression of the water-Permeable Channel Aquaporin-4 in astrocytes is regulated by Caveolin-1 phosphorylation. *Frontiers in Cellular Neuroscience*, *11*, 412. https://doi.org/10.3389/fncel.2017.00412

Boyko, M., Kuts, R., Gruenbaum, B. F., Tsenter, P., Grinshpun, J., Frank, D., Zvenigorodsky, V., Melamed, I., Brotfain, E., & Zlotnik, A. (2019). An alternative model of laser-induced stroke in the motor cortex of rats. *Biological Procedures Online*, *21*, 9. https://doi.org/10.1186/s12575-019-0097-x

Clement, T., Rodriguez-Grande, B., & Badaut, J. (2020). Aquaporins in brain edema. *Journal of Neuroscience Research*, *98*(1), 9–18. https://doi.org/10.1002/jnr.24354

Colvin, M. K., Truba, N., Sorensen, S., Henricson, E., Kinnett, K., & All Participants. (2022). Dystrophinopathy and the brain: A parent project muscular dystrophy (PPMD) meeting report November 11-12, 2021, New York City, NY. *NeuromuscDisord*, *32*(11–12), 935–944. https://doi.org/10.1016/j.nmd.2022.10.002

Enger, R., Gundersen, G. A., Haj-Yasein, N. N., Eilert-Olsen, M., Thoren, A. E., Vindedal, G. F., Petersen, P. H., Skare, Ø., Nedergaard, M., Ottersen, O. P., & Nagelhus, E. A. (2012). Molecular scaffolds underpinning macroglial polarization: An analysis of retinal Muller cells and brain astrocytes in mouse. *Glia*, *60*(12), 2018–2026. https://doi.org/10.1002/glia.22416

Fang, Y., Shi, H., Ren, R., Huang, L., Okada, T., Lenahan, C., Gamdzyk, M., Travis, Z. D., Lu, Q., Tang, L., Huang, Y., Zhou, K., Tang, J., Zhang, J., & Zhang, J. H. (2020). Pituitary adenylate cyclase-activating polypeptide attenuates brain edema by protecting blood-brain barrier and glymphatic system after subarachnoid hemorrhage in rats. *Neurotherapeutics*, *17*(4), 1954–1972. https://doi.org/10.1007/s13311-020-00925-3

Frydenlund, D. S., Bhardwaj, A., Otsuka, T., Mylonakou, M. N., Yasumura, T., Davidson, K. G., Zeynalov, E., Skare, Ø., Laake, P., Haug, F. M., Rash, J. E., Agre, P., Ottersen, O. P., & Amiry-Moghaddam, M. (2006). Temporary loss of perivascular aquaporin-4 in neocortex after transient middle cerebral artery occlusion in mice. *Proceedings of the National Academy of Sciences of the United States of America*, *103*(36), 13532–13536. https://doi.org/10.1073/pnas.0605796103

GBD 2016 Stroke Collaborators. (2019). Global, regional, and national burden of stroke, 1990-2016: a systematic analysis for the global burden of disease study 2016. *Lancet Neurology*, *18*(5), 439–458. https://doi.org/10.1016/S1474-4422(19)30034-1

Gomolka, R. S., Hablitz, L. M., Mestre, H., Giannetto, M., du, T., Hauglund, N. L., Xie, L., Peng, W., Martinez, P. M., Nedergaard, M., & Mori, Y. (2023). Loss of aquaporin-4 results in glymphatic system dysfunction via brain-wide interstitial fluid stagnation. *eLife*, *12*, 1–36. https://doi.org/10.7554/eLife.82232

Guo, Y. Z., Ma, Y. M., Zhang, X. P., Dong, L. D., Jing, L., & Zhang, J. Z. (2021). Region-specific changes in aquaporin 4 induced by hyperglycemia underlie the differences in cell swelling in the cortex and striatum after cerebral ischemia-reperfusion. *Neuroscience Letters*, *754*, 135885. https://doi.org/10.1016/j.neulet.2021.135885

Hablitz, L. M., Plá, V., Giannetto, M., Vinitsky, H. S., Stæger, F. F., Metcalfe, T., Nguyen, R., Benrais, A., & Nedergaard, M. (2020). Circadian control of brain glymphatic and lymphatic fluid flow. *Nature Communications*, *11*(1), 4411. https://doi.org/10.1038/s41467-020-18115-2

Hubbard, J. A., Hsu, M. S., Seldin, M. M., & Binder, D. K. (2015). Expression of the astrocyte Water Channel Aquaporin-4 in the mouse brain. *ASN Neuro*, *7*(5), 175909141560548. https://doi.org/10.1177/1759091415605486

Huttner, H. B., & Schwab, S. (2009). Malignant middle cerebral artery infarction: Clinical characteristics, treatment strategies, and future perspectives. *Lancet Neurology*, *8*(10), 949–958. https://doi.org/10.1016/S1474-4422(09)70224-8

Jiang, S. X., Lertvorachon, J., Hou, S. T., Konishi, Y., Webster, J., Mealing, G., Brunette, E., Tauskela, J., & Preston, E. (2005). Chlortetracycline and demeclocycline inhibit calpains and protect mouse neurons against glutamate toxicity and cerebral ischemia. *The Journal of Biological Chemistry*, *280*(40), 33811–33818. https://doi.org/10.1074/jbc.M503113200

Kitchen, P., Salman, M. M., Halsey, A. M., Clarke-Bland, C., MacDonald, J. A., Ishida, H., Vogel, H. J., Almutiri, S., Logan, A., Kreida, S., al-Jubair, T., Winkel Missel, J., Gourdon, P., Törnroth-Horsefield, S., Conner, M. T., Ahmed, Z., Conner, A. C., & Bill, R. M. (2020). Targeting Aquaporin-4 subcellular localization to treat central nervous system edema. *Cell*, *181*(4), 784–799 e719. https://doi.org/10.1016/j.cell.2020.03.037

Kuts, R., Frank, D., Gruenbaum, B. F., Grinshpun, J., Melamed, I., Knyazer, B., Tarabrin, O., Zvenigorodsky, V., Shelef, I., Zlotnik, A., & Boyko, M. (2019). A novel method for assessing cerebral edema, infarcted zone and blood-brain barrier breakdown in a single post-stroke rodent brain. *Frontiers in Neuroscience*, *13*, 1105. https://doi.org/10.3389/fnins.2019.01105

Le Roy, L., Amara, A., Le Roux, C., Bocher, O., Letondor, A., Benz, N., & Timsit, S. (2020). Principal component analysis, a useful tool to study cyclin-dependent kinase-inhibitor's effect on cerebral ischaemia. *Brain Communications*, *2*(2), fcaa136. https://doi.org/10.1093/braincomms/fcaa136

Le Roy, L., Letondor, A., Le Roux, C., Amara, A., & Timsit, S. (2021). Cellular and molecular mechanisms of R/S-Roscovitine and CDKs related inhibition under both focal and global cerebral ischemia: A focus on neurovascular unit and immune cells. *Cell*, *10*(1), 1–35. https://doi.org/10.3390/cells10010104

Li, Y., Ma, T., Zhu, X., Zhang, M., Zhao, L., Wang, P., & Liang, J. (2022). Zinc improves neurological recovery by promoting angiogenesis via the astrocyte-mediated HIF-1alpha/VEGF signaling pathway in experimental stroke. *CNS Neuroscience & Therapeutics*, *28*(11), 1790–1799. https://doi.org/10.1111/cns.13918

Lindsay, M. P., Norrving, B., Sacco, R. L., Brainin, M., Hacke, W., Martins, S., Pandian, J., & Feigin, V. (2019). World stroke organization (WSO): Global stroke fact sheet 2019. *International Journal of Stroke*, *14*(8), 806–817. https://doi.org/10.1177/1747493019881353

Lopez-Cano, M., Fernandez-Duenas, V., & Ciruela, F. (2019). Proximity ligation assay image analysis protocol: Addressing receptor-receptor interactions. *Methods in Molecular Biology*, *2040*, 41–50. https://doi.org/10.1007/978-1-4939-9686-5_3

Manley, G. T., Binder, D. K., Papadopoulos, M. C., & Verkman, A. S. (2004). New insights into water transport and edema in the central nervous system from phenotype analysis of aquaporin-4 null mice. *Neuroscience*, *129*(4), 981–989. https://doi.org/10.1016/j.neuroscience.2004.06.088

Menn, B., Bach, S., Blevins, T. L., Campbell, M., Meijer, L., & Timsit, S. (2010). Delayed treatment with systemic (S)-roscovitine provides neuroprotection and inhibits in vivo CDK5 activity increase in animal stroke models. *PLoS One*, *5*(8), e12117. https://doi.org/10.1371/journal.pone.0012117

Mestre, H., Hablitz, L. M., Xavier, A. L., Feng, W., Zou, W., Pu, T., Monai, H., Murlidharan, G., Castellanos Rivera, R. M., Simon, M. J.,

Pike, M. M., Plá, V., du, T., Kress, B. T., Wang, X., Plog, B. A., Thrane, A. S., Lundgaard, I., Abe, Y., … Nedergaard, M. (2018). Aquaporin-4-dependent glymphatic solute transport in the rodent brain. *eLife*, *7*, 1–31. https://doi.org/10.7554/eLife.40070

Michinaga, S., & Koyama, Y. (2015). Pathogenesis of brain edema and investigation into anti-edema drugs. *International Journal of Molecular Sciences*, *16*(5), 9949–9975. https://doi.org/10.3390/ijms16059949

Murata, Y., Sugimoto, K., Yang, C., Harada, K., Gono, R., Harada, T., Miyashita, Y., Higashisaka, K., Katada, R., Tanaka, J., & Matsumoto, H. (2020). Activated microglia-derived macrophage-like cells exacerbate brain edema after ischemic stroke correlate with astrocytic expression of aquaporin-4 and interleukin-1 alpha release. *Neurochemistry International*, *140*, 104848. https://doi.org/10.1016/j.neuint.2020.104848

Nakada, T. (2014). Virchow-Robin space and aquaporin-4: New insights on an old friend. *Croatian Medical Journal*, *55*(4), 328–336. https://doi.org/10.3325/cmj.2014.55.328

Neely, J. D., Amiry-Moghaddam, M., Ottersen, O. P., Froehner, S. C., Agre, P., & Adams, M. E. (2001). Syntrophin-dependent expression and localization of Aquaporin-4 water channel protein. *Proceedings of the National Academy of Sciences of the United States of America*, *98*(24), 14108–14113. https://doi.org/10.1073/pnas.241508198

Ort, T., Voronov, S., Guo, J., Zawalich, K., Froehner, S. C., Zawalich, W., & Solimena, M. (2001). Dephosphorylation of beta2-syntrophin and Ca2+/mu-calpain-mediated cleavage of ICA512 upon stimulation of insulin secretion. *The EMBO Journal*, *20*(15), 4013–4023. https://doi.org/10.1093/emboj/20.15.4013

Patabendige, A., & Chen, R. (2022). Astrocytic aquaporin 4 subcellular translocation as a therapeutic target for cytotoxic edema in ischemic stroke. *Neural Regeneration Research*, *17*(12), 2666–2668. https://doi.org/10.4103/1673-5374.339481

Patabendige, A., Singh, A., Jenkins, S., Sen, J., & Chen, R. (2021). Astrocyte activation in neurovascular damage and repair following ischaemic stroke. *International Journal of Molecular Sciences*, *22*(8), 1–22. https://doi.org/10.3390/ijms22084280

Peters, M. F., Adams, M. E., & Froehner, S. C. (1997). Differential association of syntrophin pairs with the dystrophin complex. *The Journal of Cell Biology*, *138*(1), 81–93. https://doi.org/10.1083/jcb.138.1.81

Ren, Z., Iliff, J. J., Yang, L., Yang, J., Chen, X., Chen, M. J., Giese, R. N., Wang, B., Shi, X., & Nedergaard, M. (2013). 'Hit & Run' model of closed-skull traumatic brain injury (TBI) reveals complex patterns of post-traumatic AQP4 dysregulation. *Journal of Cerebral Blood Flow and Metabolism*, *33*(6), 834–845. https://doi.org/10.1038/jcbfm.2013.30

Risher, W. C., Andrew, R. D., & Kirov, S. A. (2009). Real-time passive volume responses of astrocytes to acute osmotic and ischemic stress in cortical slices and in vivo revealed by two-photon microscopy. *Glia*, *57*(2), 207–221. https://doi.org/10.1002/glia.20747

Rousselet, E., Letondor, A., Menn, B., Courbebaisse, Y., Quille, M. L., & Timsit, S. (2018). Sustained (S)-roscovitine delivery promotes neuroprotection associated with functional recovery and decrease in brain edema in a randomized blind focal cerebral ischemia study. *Journal of Cerebral Blood Flow and Metabolism*, *38*(6), 1070–1084. https://doi.org/10.1177/0271678X17712163

Schubert, S., Knoch, K. P., Ouwendijk, J., Mohammed, S., Bodrov, Y., Jäger, M., Altkrüger, A., Wegbrod, C., Adams, M. E., Kim, Y., Froehner, S. C., Jensen, O. N., Kalaidzidis, Y., & Solimena, M. (2010). beta2-Syntrophin is a Cdk5 substrate that restrains the motility of insulin secretory granules. *PLoS One*, *5*(9), e12929. https://doi.org/10.1371/journal.pone.0012929

Simard, J. M., Kent, T. A., Chen, M., Tarasov, K. V., & Gerzanich, V. (2007). Brain oedema in focal ischaemia: Molecular pathophysiology and theoretical implications. *Lancet Neurology*, *6*(3), 258–268. https://doi.org/10.1016/S1474-4422(07)70055-8

Simon, M., Wang, M. X., Ismail, O., Braun, M., Schindler, A. G., Reemmer, J., Wang, Z., Haveliwala, M. A., O'Boyle, R. P., Han, W. Y., Roese, N., Grafe, M., Woltjer, R., Boison, D., & Iliff, J. J. (2022). Loss of perivascular aquaporin-4 localization impairs glymphatic exchange and promotes amyloid beta plaque formation in mice. *Alzheimer's Research & Therapy*, *14*(1), 59. https://doi.org/10.1186/s13195-022-00999-5

Søren Nielsen, E. A. N., Amiry-Moghaddam, M., Bourque, C., Agre, P., & Ottersen, O. P. (1997). Specialized membrane domains for water transport in glial cells. *The Journal of Neuroscience*, *17*, 171–180.

Stokum, J. A., Gerzanich, V., & Simard, J. M. (2016). Molecular pathophysiology of cerebral edema. *Journal of Cerebral Blood Flow and Metabolism*, *36*(3), 513–538. https://doi.org/10.1177/0271678X15617172

Sutherland, B. A., Neuhaus, A. A., Couch, Y., Balami, J. S., DeLuca, G. C., Hadley, G., Harris, S. L., Grey, A. N., & Buchan, A. M. (2016). The transient intraluminal filament middle cerebral artery occlusion model as a model of endovascular thrombectomy in stroke. *Journal of Cerebral Blood Flow and Metabolism*, *36*(2), 363–369. https://doi.org/10.1177/0271678X15606722

Sylvain, N. J., Salman, M. M., Pushie, M. J., Hou, H., Meher, V., Herlo, R., Peeling, L., & Kelly, M. E. (2021). The effects of trifluoperazine on brain edema, aquaporin-4 expression and metabolic markers during the acute phase of stroke using photothrombotic mouse model. *Biochimica et Biophysica Acta – Biomembranes*, *1863*(5), 183573. https://doi.org/10.1016/j.bbamem.2021.183573

Verkman, A. S., Smith, A. J., Phuan, P. W., Tradtrantip, L., & Anderson, M. O. (2017). The aquaporin-4 water channel as a potential drug target in neurological disorders. *Expert Opinion on Therapeutic Targets*, *21*(12), 1161–1170. https://doi.org/10.1080/14728222.2017.1398236

Wali, B., Ishrat, T., Atif, F., Hua, F., Stein, D. G., & Sayeed, I. (2012). Glibenclamide administration attenuates infarct volume, hemispheric swelling, and functional impairments following permanent focal cerebral ischemia in rats. *Stroke Research and Treatment*, *2012*, 460909. https://doi.org/10.1155/2012/460909

Wang, M., Iliff, J. J., Liao, Y., Chen, M. J., Shinseki, M. S., Venkataraman, A., & Nedergaard, M. (2012). Cognitive deficits and delayed neuronal loss in a mouse model of multiple microinfarcts. *The Journal of Neuroscience*, *32*(50), 17948–17960. https://doi.org/10.1523/JNEUROSCI.1860-12.2012

Wu, S., Yuan, R., Wang, Y., Wei, C., Zhang, S., Yang, X., Wu, B., & Liu, M. (2018). Early prediction of malignant brain edema after ischemic stroke. *Stroke*, *49*(12), 2918–2927. https://doi.org/10.1161/STROKEAHA.118.022001

Zelenina, M. (2010). Regulation of brain aquaporins. *Neurochemistry International*, *57*(4), 468–488. https://doi.org/10.1016/j.neuint.2010.03.022

SUPPORTING INFORMATION

Additional supporting information can be found online in the Supporting Information section at the end of this article.

How to cite this article: Moëlo, C., Quillévéré, A., Le Roy, L., & Timsit, S. (2024). (S)-roscovitine, a CDK inhibitor, decreases cerebral edema and modulates AQP4 and α1-syntrophin interaction on a pre-clinical model of acute ischemic stroke. *Glia*, *72*(2), 322–337. https://doi.org/10.1002/glia.24477